A Simplified Cartesian Basis Model for Intrapolyad Emission Intensities in the Bent-to-linear Electronic Transition of Acetylene

G. Barratt Park,[1, a)] Adam H. Steeves,[1, 2] Joshua H. Baraban,[1, 3] and Robert W. Field[1]

[1)] *Department of Chemistry, Massachusetts Institute of Technology, Cambridge, Massachusetts 02139*

[2)] *Current Address: Department of Chemistry, Ithaca College, Ithaca, NY 14850*

[3)] *Current Address: Department of Chemistry and Biochemistry, University of Colorado Boulder, Boulder, CO 80309-0215*

The acetylene emission spectrum from the *trans*-bent electronically excited $\tilde{A}$ state to the linear ground electronic $\tilde{X}$ state has attracted considerable attention because it grants Franck-Condon access to local bending vibrational levels of the $\tilde{X}$ state with large-amplitude motion along the acetylene $\rightleftharpoons$ vinylidene isomerization coordinate. For emission from the ground vibrational level of the $\tilde{A}$ state, there is a simplifying set of Franck-Condon propensity rules that gives rise to *only one* zero-order bright state per conserved vibrational polyad of the $\tilde{X}$ state. Unfortunately, when the upper level involves excitation in the highly admixed *ungerade* bending modes, ν_4' and ν_6', the simplifying Franck-Condon propensity rule breaks down—so long as the usual polar basis (with v and l quantum numbers) is used to describe the degenerate bending vibrations of the $\tilde{X}$ state—and the intrapolyad intensities result from complicated interference patterns between many zero-order bright states. In this paper, we show that when the degenerate bending levels are instead treated in the Cartesian two-dimensional harmonic oscillator basis (with v_x and v_y quantum numbers), the propensity for *only one* zero-order bright state (in the Cartesian basis) is *restored*, and the intrapolyad intensities are simple to model, so long as corrections are made for anharmonic interactions. As a result of $trans \rightleftharpoons cis$ isomerization in the $\tilde{A}$ state, intrapolyad emission patterns from overtones of ν_4' and ν_6' evolve as quanta of *trans* bend (ν_3') are added, so the emission intensities are not only relevant to the ground-state acetylene $\rightleftharpoons$ vinylidene isomerization—they are also a direct reporter of isomerization in the electronically-excited state.

[a)]Electronic mail: barratt@mit.edu, barratt.park@gmail.com

I. INTRODUCTION

The bending dynamics of acetylene on both its ground ($\tilde{X}\ ^1\Sigma_g^+$) and first singlet excited ($\tilde{A}\ ^1A_u$) electronic states have attracted considerable spectroscopic and theoretical attention. Acetylene has a linear equilibrium geometry in the $\tilde{X}$ state but becomes *trans*-bent upon excitation to the $\tilde{A}$ electronic state. Although acetylene was the first molecule for which a qualitative change in geometry and symmetry accompanying an electronic excitation was proven by spectroscopic methods,[1–3] similar large amplitude displacements along bending coordinates are known to be quite common in the electronic spectroscopy of π-bonded molecules. Qualitative changes in bond angles and geometries are expected to result whenever an electronic $\pi^* \leftarrow \pi$ excitation changes the effective bond order and the accompanying sp^n hybridization.

Because acetylene is the prototype molecule for CC triple bond systems, its dynamics are of broad interest to the chemical community. Significant work has been done to characterize the acetylene $\rightleftharpoons$ vinylidene and *trans* $\rightleftharpoons$ *cis* isomerization reactions that occur on the $\tilde{X}$ and $\tilde{A}$ electronic surfaces, respectively. Both of these reactions primarily involve bending vibrations. Because the $\tilde{A}$–$\tilde{X}$ transition involves a large change in equilibrium bond angles, the electronic transition grants Franck-Condon (FC) access to high overtones of the bending vibrations on both electronic surfaces, which has allowed extensive characterization of large amplitude bending dynamics relevant to chemical isomerization.[4,5] Investigators have used a variety of spectroscopic schemes to observe these levels, including laser-induced fluorescence (LIF),[5–11] dispersed fluorescence (DF),[12–15] and Stimulated Emission Pumping (SEP).[16,17]

One phenomenon of particular interest is the emergence of vibrational eigenstates on the $\tilde{X}$ electronic surface that have large amplitude local bending character (i.e. with the bending amplitude localized in a single CCH bend), because this vibrational motion lies approximately along the acetylene $\rightleftharpoons$ vinylidene minimum energy isomerization path.[18,19] Excited bending levels of the $\tilde{A}$ state may provide Franck-Condon access (via DF or SEP) to isomerization-relevant levels of the $\tilde{X}$ state, because the half-linear transition state geometry of the *trans* $\rightleftharpoons$ *cis* isomerization in the $\tilde{A}$ state[20] is believed to resemble the acetylene $\rightleftharpoons$ vinylidene transition state geometry.[21–23] This has motivated a recent full-dimensional calculation of Franck-Condon factors in the harmonic normal mode basis.[24,25] The results of the harmonic calculation indicate that $\tilde{A}$-state levels with high quanta of torsion (ν_4') and

cis-bend (ν_6') excitation provide good FC overlap with large-amplitude counter-rotational and local bending zero-order bright states, respectively, of the $\tilde{\mathrm{X}}$ state. However, the results of Refs. 24 and 25 provide only qualitative—not quantitative—agreement with experiment, largely because the treatment fails to account for anharmonic interactions that occur in the $\tilde{\mathrm{A}}$ state.

In this paper, we correct for interactions among bending levels of the $\tilde{\mathrm{A}}$ state and obtain near-quantitative agreement with the patterns observed in DF and SEP spectra. Furthermore, we demonstrate that within sets of pure bending polyads of the $\tilde{\mathrm{X}}$ state with conserved total number of bending quanta, $v_4'' + v_5''$, the emission intensity patterns are correctly explained by a simple Franck-Condon propensity rule in the Cartesian basis for the degenerate two-dimensional harmonic oscillator (2DHO) bending wavefunctions of the linear $\tilde{\mathrm{X}}$ state. These propensities are analogous to those that are naturally applied in the case of nonlinear symmetric-to-asymmetric top transitions.

II. POLYAD STRUCTURE AND BENDING DYNAMICS IN THE $\tilde{\mathrm{A}}$—$\tilde{\mathrm{X}}$ SYSTEM

Descriptions and frequencies of the acetylene $\tilde{\mathrm{X}}$-state normal modes are given in Table I. The vibrational Hamiltonian of the $\tilde{\mathrm{X}}$ state of acetylene is approximately block diagonal in the polyad-forming quantum numbers, $\{N_\mathrm{s}, N_\mathrm{res}, l\}$:

$$N_s = v_1'' + v_2'' + v_3'' \tag{1}$$

$$N_\mathrm{res} = 5v_1'' + 3v_2'' + 5v_3'' + v_4'' + v_5'' \tag{2}$$

$$l = l_4 + l_5, \tag{3}$$

up to energies of at least 15,000 cm^{-1}.[4,12,13,26–29] In other words, zero-order vibrational levels with the same polyad quantum numbers may interact with one another, but do not interact with levels belonging to other polyads. The N_s quantum number conserves the total quanta of stretching excitation, and the l quantum number conserves the total quanta of vibrational angular momentum from the bending modes. The N_{res} quantum number is approximately proportional to the vibrational energy and arises from near-integer ratios between the mode frequencies that lead to resonances. In addition to the polyad numbers, $\{N_\mathrm{s}, N_\mathrm{res}, l\}$, the

TABLE I. Normal mode labels for $\tilde{\mathrm{X}}$-state acetylene. The harmonic vibrational frequencies (taken from ref. 29) were determined from experiment after deperturbing the anharmonic resonances.

Mode	Description	Symmetry	ω/cm^{-1}
ν_1''	symmetric stretch	σ_g^+	3397.12
ν_2''	CC stretch	σ_g^+	1981.80
ν_3''	antisymmetric stretch	σ_u^+	3316.86
ν_4''	*trans* bend	π_g	608.73
ν_5''	*cis* bend	π_u	729.08

vibrational levels also have well-defined g/u symmetry and may be symmetrized to have well-defined $+/-$ total parity. The parity and g/u symmetry are conserved by the vibrational Hamiltonian, and are therefore also conserved within each polyad. In this paper, we will use the term "polyad set" to mean the set of polyads with given values of $\{N_s, N_{res}\}$, which may differ in l, g/u symmetry, and $+/-$ total parity. In the absence of excitation in the stretching modes, $N_s = 0$ and the bending modes $\nu_4''(\pi_g)$ and $\nu_5''(\pi_u)$ form *pure bending* polyads with conserved polyad numbers

$$N_B = N_{\mathrm{res}} = v_4'' + v_5'' \tag{4}$$

$$l = l_4 + l_5. \tag{5}$$

At high quanta of bending excitation ($N_B \geq 12$), the ν_4'' and ν_5'' normal modes become strongly mixed via intra-polyad Darling-Dennison interactions, and local bending quantum numbers provide a better zero-order description of the vibrational eigenstates.[18,19]

Descriptions and frequencies of the $\tilde{\mathrm{A}}$-state normal modes are given in Table II. A global rovibrational effective Hamiltonian fit has not been attempted for the $\tilde{\mathrm{A}}$ state, but a polyad model has been used for the near-degenerate torsion $\nu_4'(\mathrm{a}_u)$ and *cis*-bending $\nu_6'(\mathrm{b}_u)$ modes, which interact via Darling-Dennison resonances and *a*- and *b*-axis Coriolis interactions. In this paper, we refer to polyads with $v_4' + v_6' = n$ as B^n.

III. FRANCK-CONDON PROPENSITY RULES IN THE CARTESIAN BASIS

The ν_6' (*cis*-bend) and ν_4' (torsion) vibrational modes that comprise the $\tilde{\mathrm{A}}$-state B^n polyads correlate to the in-plane and out-of-plane components of the ν_5'' (*cis*-bend) vibration

TABLE II. Normal mode labels for $\tilde{\mathrm{A}}$-state acetylene. The harmonic vibrational frequencies (taken from ref. 11) were determined from experiment after deperturbing the anharmonic resonances.

Mode	Description	Symmetry	ω/cm^{-1}
ν_1'	symmetric stretch	a_g	3052.1
ν_2'	CC stretch	a_g	1420.9
ν_3'	*trans* bend	a_g	1098.0
ν_4'	torsion	a_u	787.7
ν_5'	antisymmetric stretch	b_u	3032.4
ν_6'	*cis* bend	b_u	801.6

in the $\tilde{\mathrm{X}}$ state. Because the frequencies of ν_6' and ν_4' are nearly degenerate and are close to the ν_5'' frequency and because there is no displacement along the *ungerade cis*-bend vibrational mode between the equilibrium geometries of the $\tilde{\mathrm{X}}$ and $\tilde{\mathrm{A}}$ states, there is a Franck-Condon propensity for quanta in these modes to be conserved in the $\tilde{\mathrm{A}}$–$\tilde{\mathrm{X}}$ transition. That is, there is a vibrational propensity for transitions between levels with $v_5'' = v_4' + v_6'$ to be strongly allowed, but for transitions between vibrational levels with $v_5'' \neq v_4' + v_6'$ to be much weaker. This propensity is well established,[4,12,30] and similar arguments that stem from the near-equal CH bond lengths in the $\tilde{\mathrm{X}}$ and $\tilde{\mathrm{A}}$ states lead to FC propensities conserving the quanta of symmetric and antisymmetric CH stretch, $v_1'' = v_1'$ and $v_3'' = v_5'$, respectively. This leads to a simplifying golden rule that has long guided our understanding of the emission spectrum of acetylene: emission from $\tilde{\mathrm{A}}$-state levels *with no excitation in the B^n polyads* will lead to *only one* zero order bright state within each $\tilde{\mathrm{X}}$-state polyad. That is, an $\tilde{\mathrm{A}}$-state vibrational level with vibrational quantum numbers $(v_1', v_2', v_3', v_4' = 0, v_5', v_6' = 0)$ will have a strong propensity to fluoresce to the zero-order bright state within each $\tilde{\mathrm{X}}$-state polyad (with given values of $\{N_s, N_{\mathrm{res}}, l\}$) with quantum numbers

$$\begin{aligned} v_1'' &= v_1', \quad v_2'' = N_s - v_1' - v_5', \\ v_3'' &= v_5', \quad v_4'' = N_{\mathrm{res}} - 5v_1' - 3v_2' - 5v_3', \\ l_4 &= l, \quad\quad v_5'' = l_5 = 0. \end{aligned} \tag{6}$$

Intrapolyad interactions described by the global effective Hamiltonian will fractionate the single zero-order bright state (6) between the eigenstates of the polyad in a manner that is well understood.[15,29]

On the other hand, in emission experiments from $\tilde{\text{A}}$-state vibrational levels with excitation in the B^n polyads, previous investigators—who have used the conventional basis of polar $|v, l\rangle$ quantum numbers to label the degenerate linear molecule bending (2DHO) wavefunctions—have observed *multiple* zero-order bright states within a given $\tilde{\text{X}}$-state polyad with different combinations of $l_4 + l_5 = l$.[15,31] The observed emission pattern within each $\tilde{\text{X}}$-state polyad will result from interferences that arise when the multiple zero-order states are fractionated among the eigenstates of the polyad. The SEP and DF spectra in Figure 1 from the three $K' = 1$ members of the $\tilde{\text{A}}$-state 3^2B^2 polyad to the $N_B = 10$ pure bending polyad of the $\tilde{\text{X}}$ state illustrate this point. Each member of the 3^2B^2 polyad gives rise to a qualitatively different pattern of intensities that are distributed across the polyad set. Because many quanta of both v_4'' and v_5'' are required to form large-amplitude local bender levels relevant to the acetylene $\rightleftharpoons$ vinylidene isomerization, it is important to understand the emission intensities from B^n polyads. This was a large part of the motivation for our recent full-dimensional FC calculation.[24,25]

In complement to previous work, we show that—when the $\tilde{\text{X}}$-state bending modes ν_4'' and ν_5'' are viewed in the basis of *Cartesian* doubly degenerate 2DHOs with in-plane (y) and out-of-plane (x) bending quanta—there are additional, stricter, Franck-Condon propensities that require conservation of the number of in-plane vs. out-of-plane *cis* bend quanta. That is, there is a strong propensity for

$$v_{5x}'' = v_4', \quad v_{5y}'' = v_6'. \tag{7}$$

Also, because the out-of-plane component of ν_4'' correlates with a rotation in the *trans*-bent $\tilde{\text{A}}$-state, the $\tilde{\text{A}}$-state Eckart conditions prevent ν_{4x}'' from participating in the *vibrational* FC overlap intensities. This leads to the additional Cartesian propensity, $v_{4x}'' = 0$. This Eckart restriction is explained in detail in Ref. 24, and is based on considerations for linear-to-bent transitions that were first utilized by Kovner *et al.*[32] and later described in detail by Watson.[33,34] However, the work of Kovner and Watson was limited to systems where only one bending vibration was considered, so these authors did not explore the multidimensional bending dynamics encoded by bright states that arise from linear-to-bent transitions in polyatomic molecules.

The advantage of applying these stricter Cartesian-basis propensity rules is that in the

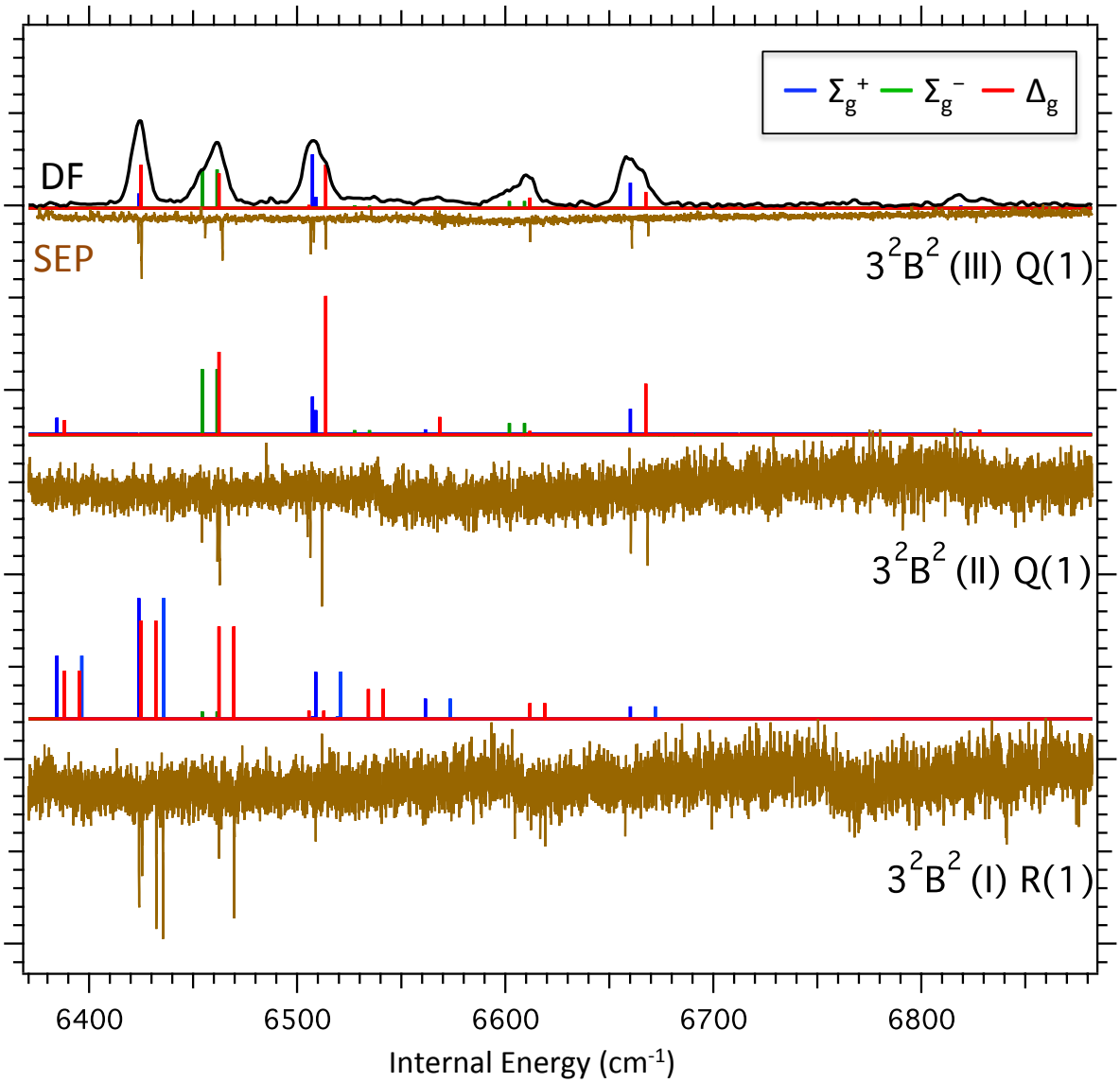

FIG. 1. The SEP spectra from $J' = 1$ intermediate levels of the three different $K' = 1$ stacks of the 3^2B^2 polyad of the $\tilde{A}$ state (labeled with Roman numerals in order of increasing energy) into the $\{N_s, N_{res}\} = \{0, 10\}$ pure bending polyad set of the $\tilde{X}$ state are displayed as downward-directed peaks. The eigenstate compositions of the SEP intermediates are given in Table IV. The DF spectrum from 3^2B^2 $K' = 1$ Q(1) is shown for comparison at the top of the figure. Also shown as upward stick spectra are the polyad set intensities obtained from the Cartesian propensity model. The stick spectrum is colored according to the symmetry of the lower level (see legend).

new basis there is *only one* zero-order state within a given $\tilde{X}$-state polyad that is bright in emission from *any* zero-order level of the $\tilde{A}$ state, including those with excitation in the members of the B^n polyads. Thus, when the bright state is viewed in the Cartesian basis, there is no interference. An $\tilde{A}$-state level with vibrational quantum numbers $(v_1', v_2', v_3', v_4', v_5', v_6')$ will

have a propensity to fluoresce to the member of a given $\tilde{\mathrm{X}}$-state polyad set with quantum numbers

$$\begin{aligned} v_1'' &= v_1', \quad v_2'' = N_s - v_1' - v_5', \\ v_3'' &= v_5', \quad v_{4y}'' = N_{\mathrm{res}} - 5v_1' - 3v_2' - 5v_3' - v_4' - v_6', \\ v_{4x}'' &= 0, \quad v_{5x}'' = v_4', \quad v_{5y}'' = v_6'. \end{aligned} \tag{8}$$

Bright states of the type given in Eq. (8) represent a well-defined linear combination of degenerate 2DHO states in the polar basis with quantum numbers $|v_4^{(l_4)}, v_5^{(l_5)}\rangle$, which is the basis in which the $\tilde{\mathrm{X}}$-state global effective Hamiltonian is written.[15,29,35] The Cartesian-to-polar transformation (in the signed-l product basis of ν_4'' and ν_5'') is obtained by standard ladder operator methods:

$$\begin{aligned} |v_4^{l_4}, v_5^{l_5}\rangle = &\left[(n_{4d})!\,(n_{4g})!\,(n_{5d})!\,(n_{5g})!\right]^{-1/2} \\ &\times \left(\hat{a}_{4x}^\dagger + i\hat{a}_{4y}^\dagger\right)^{n_{4d}} \left(\hat{a}_{4x}^\dagger - i\hat{a}_{4y}^\dagger\right)^{n_{4g}} \\ &\times \left(\hat{a}_{5x}^\dagger + i\hat{a}_{5y}^\dagger\right)^{n_{5d}} \left(\hat{a}_{5x}^\dagger - i\hat{a}_{5y}^\dagger\right)^{n_{5g}} |0,0\rangle|0,0\rangle, \end{aligned} \tag{9}$$

where

$$\begin{aligned} n_{4d} &= \frac{1}{2}(v_4 + l_4), \quad n_{4g} = \frac{1}{2}(v_4 - l_4), \\ n_{5d} &= \frac{1}{2}(v_5 + l_4), \quad n_{5g} = \frac{1}{2}(v_5 - l_5). \end{aligned}$$

The terms in the expansion of Eq. (9) are evaluated according to

$$\begin{aligned} &(\hat{a}_{4x}^\dagger)^{v_{4x}} (\hat{a}_{4y}^\dagger)^{v_{4y}} (\hat{a}_{5x}^\dagger)^{v_{5x}} (\hat{a}_{5y}^\dagger)^{v_{5y}} |0,0\rangle|0,0\rangle \\ &\qquad = \left(v_{4x}! v_{4y}! v_{5x}! v_{5y}!\right)^{1/2} |v_{4x}, v_{4y}\rangle|v_{5x}, v_{5y}\rangle. \end{aligned} \tag{10}$$

The $|v_4^{(l_4)}, v_5^{(l_5)}\rangle$ basis functions must be symmetrized to form states of well-defined vibrational parity:

$$|v_4^{(l_4)}, v_5^{(l_5)}\rangle^{\pm} = \frac{1}{\sqrt{2}} \left(|v_4^{(l_4)}, v_5^{(l_5)}\rangle \pm |v_4^{(-l_4)}, v_5^{(-l_5)}\rangle\right). \tag{11}$$

Because of the $K' - l'' = \pm 1$ rotational selection rule for the c-type transition moment, only a handful of terms from Eq. (9) must be evaluated to obtain the desired transformation. The basis transformation coefficients have asymptotically limiting behavior as N_B increases. For example, in Figure 2, the Cartesian overlap coefficients are shown for emission from the a_g members of B^2 upper levels to the various classes of pure-bending bright states, as

a function of N_B. Note that the overlaps from the in-plane 6^2 vibrational level and the out-of-plane 4^2 vibrational level are identical in magnitude, but have a *phase relationship* that gives rise to *qualitatively different* bending dynamics and spectral intensity patterns.[25] From the correlation table connecting $D_{\infty h}$ to C_{2h}, we find that in emission to $l = 0$ levels of

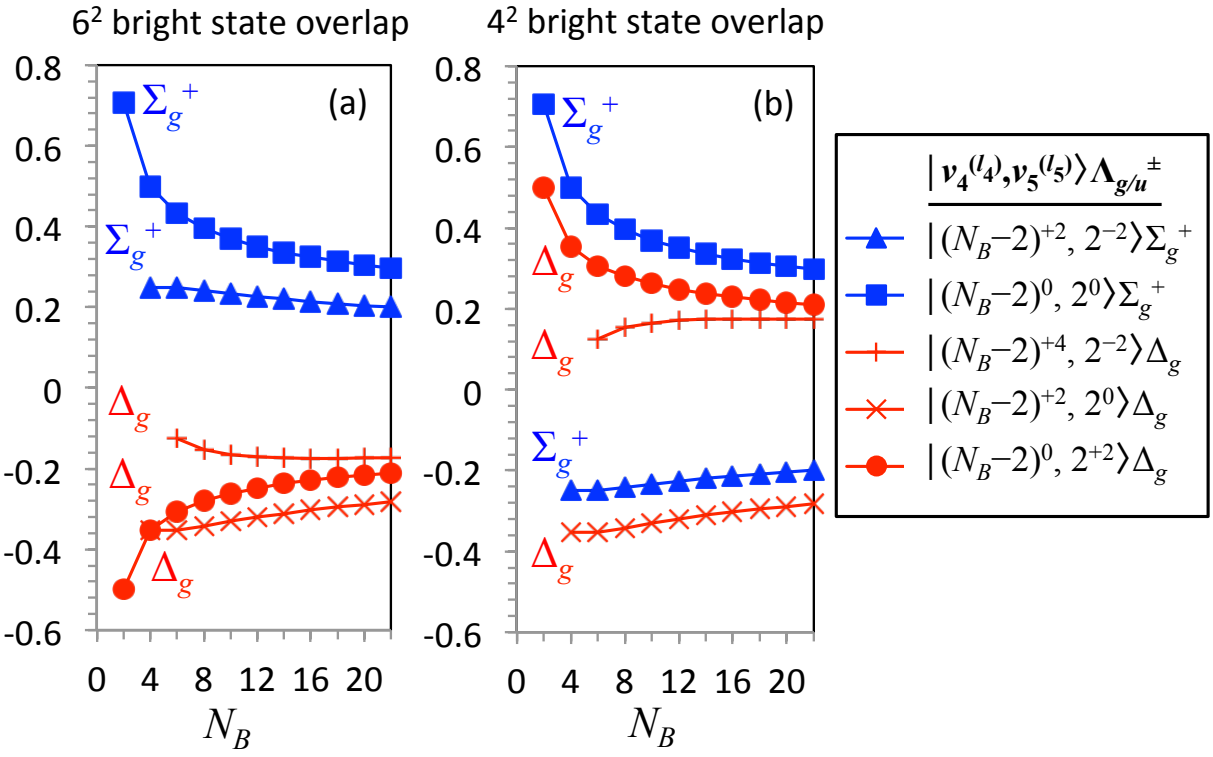

FIG. 2. Overlap of the zero-order Cartesian bright states $|v''_{4x}, v''_{4y}\rangle|v''_{5x}, v''_{5y}\rangle = |0, N_B - 2\rangle|0, 2\rangle$ (panel a) and from $|0, N_B - 2\rangle|2, 0\rangle$ (panel b)—which are accessed from 6^2 and 4^2, respectively—with the $l = 0, 2$ zero-order polar 2DHO basis states. The various classes of polar basis bright states are indicated in the legend. The magnitude of overlap does not depend on which Cartesian plane of ν''_5 is excited. However, the different pattern of phases that is obtained from either plane encodes a qualitatively different spectral interference pattern from 6^n vs. 4^n (as in Figure 1) and qualitatively different bending dynamics (see Figures 3 and 4 of Ref. 25).

the $\tilde{X}$-state, the vibrational selection rules are $a_g \rightarrow \sigma_g^+$, $b_g \rightarrow \sigma_g^-$, $a_u \rightarrow \sigma_u^-$, and $b_u \rightarrow \sigma_u^+$.

IV. CORRECTIONS FOR ANHARMONIC INTERACTIONS

In the current work, we use the $\tilde{X}$-state global effective Hamiltonian parameters of Ref. 15 to obtain the fractionation of zero-order basis states obtained from Eq. (8) into the

eigenstates on the $\tilde{X}$ electronic surface. Although a global effective Hamiltonian fit has not been reported for the $\tilde{A}$ state, considerable effort has been made to characterize the vibrational structure and most of the B^n intrapolyad interactions are understood up to 5000 cm^{-1} above the $\tilde{A}$-state origin.[5–8,10,36] The individual polyad fit models (using the complex matrix elements defined in Eq. 8 of Ref. 8) can be used to obtain the correctly phased linear combination of zero-order bright states given in Eq. (8). Tables III and IV list the zero-order contributions to the specific eigenstates of the 3^2B^1, 3^3B^1, and 3^2B^2 polyads whose emission spectra are modeled in Section V. In Section V, the b-axis Coriolis interaction with the $K' = 0$ levels is neglected, because it is a small effect and any $K' = 0$ character that results will fluoresce to $\tilde{X}$-state polyads with $l = 1$.

TABLE III. Eigenenergies (in cm^{-1}) and basis state coefficients for the nominally 3^n6^1 $J_{K_aK_c} = 1_{10}$ upper levels used to obtain the DF spectra reported in Ref. 15. The coefficients are obtained from the fit parameters for a- and b-axis Coriolis interactions given in Refs. 6 and 7.

zero-order		$n = 2$	$n = 3$
vib. level	$J_{K_aK_c}$	44972.36	45941.07
3^n6^1	1_{10}	$-0.841i$	$-0.938i$
3^n4^1	1_{01}	0.036	0.027
	1_{11}	0.539	0.345

TABLE IV. Eigenenergies (in cm^{-1}) and basis state coefficients for the three $K' = 1$ levels of the 3^2B^2 used as the upper level for the SEP spectra in Figure 1. The levels are labeled with Roman numerals in order of increasing energy. The R(0) and Q(1) transitions used in the PUMP terminate on levels of opposite total rovibronic parity.

zero-order		(I) R(0)	(II) Q(1)	(III) Q(1)
vib. level	$J_{K_aK_c}$	45728.12	45728.20	45812.77
$3^24^2(a_g)$	1_{01}		$0.054i$	0.035
	1_{11}		$0.63i$	0.74
	1_{10}	0.19		
$3^24^16^1(b_g)$	1_{01}	$0.021i$		
	1_{11}	$0.25i$		
	1_{10}		0.77	$-0.59i$
$3^26^2(a_g)$	1_{01}		$-0.0013i$	-0.016
	1_{11}		$0.078i$	-0.31
	1_{10}	0.95		

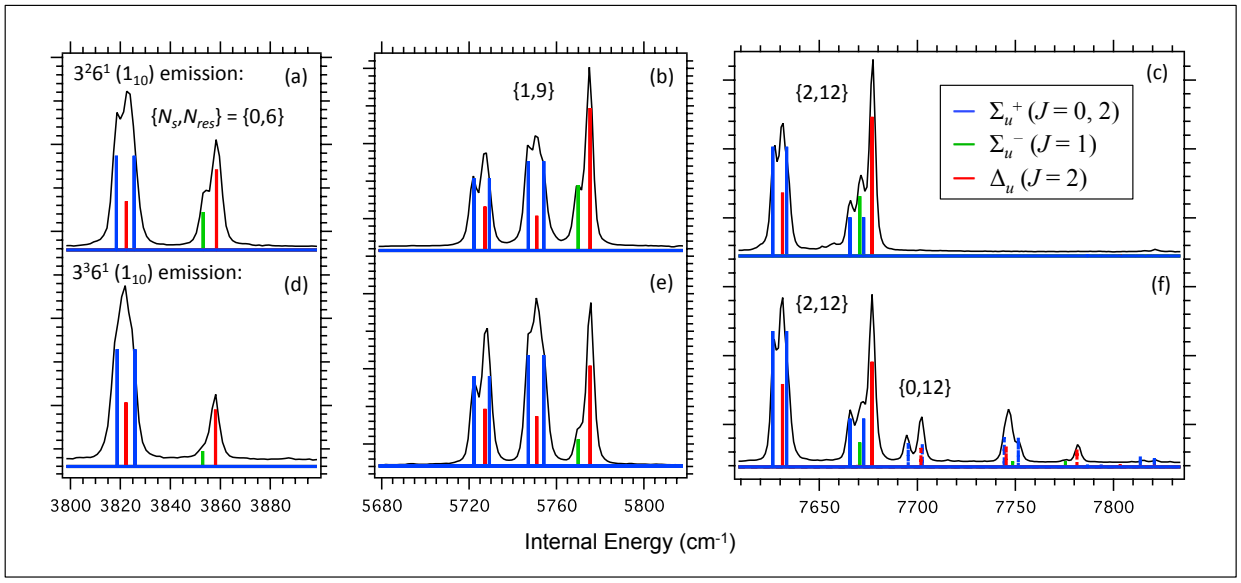

FIG. 3. High-resolution DF spectra obtained from $J_{K_aK_c} = 1_{10}$ rotational levels of 3^26^1 and 3^36^1 into a representative collection of pure-bend and stretch-bend polyad sets. The DF spectra have been previously reported in Ref. 15, and the eigenstate compositions of the upper levels are given in Table III. Stick spectra show the relative intensities obtained from the Cartesian propensity model, colored according to the symmetry of the lower state. In panels (c) and (d), the modeled intensities into the polyad sets $\{N_s, N_{res}\} = \{2, 12\}$ and $\{0, 12\}$ are scaled by the relative Franck-Condon factors reported in Ref. 15.

V. COMPARISON OF MEASURED EMISSION INTENSITY PATTERNS WITH THE CARTESIAN BRIGHT STATE MODEL

Figure 3 provides a comparison between the high resolution DF spectra obtained from the $J_{K_aK_c} = 1_{10}$ rotational level of the 3^26^1 and 3^36^1 (Ref. 15) and the Cartesian propensity model developed in Section III. The zero-order members of the B^1 polyad are almost exactly degenerate and the eigenstates are strongly mixed by a- and b-axis Coriolis interactions.[6] However, because modes ν_3' and ν_6' combine to form the reaction coordinate for the *trans* $\rightleftharpoons$ *cis* isomerization, there is a large negative x_{36} cross-anharmonicity that encodes the softening of the potential energy surface along the approach to the barrier.[5] In the combination polyads, 3^nB^1, the addition of mode ν_3' causes a much larger decrease in the effective ν_6' frequency than in the effective ν_4' frequency. As a result, the zero-order 3^n6^1 levels are detuned from resonance, and the mixing angle of zero-order 3^n4^1 into the nominally 3^n6^1 eigenstate decreases with increasing n (see Table III).

The model captures several clear differences between the intrapolyad intensity patterns

in Figure 3 that result from the evolution of the $3^n B^1$ polyad structure. First, because the symmetry of $3^n 4^1(a_u)$ correlates to Σ_u^- and the symmetry of $3^n 6^1(b_u)$ correlates to Σ_u^+, the relative intensity of transitions to Σ_u^- levels is a direct measurement of the a_u character of the upper level. There is a ~ 2 fold decrease in the relative intensity of Σ_u^- levels when the upper level is changed from $3^2 6^1$ to $3^3 6^1$, which is consistent with the decreased admixture of $3^n 4^1$ character from *a*-axis Coriolis effects in the upper level. Similar arguments are used by the authors of Ref. 5 to determine the a_g vs. b_g character of the members of $3^2 B^2$ from the appearance of Σ_g^- peaks in the SEP spectrum.

On the other hand, Δ_u correlates with $a_u + b_u$, so the intensities of transitions to Δ_u levels in Figure 3 arise from *interferences* between the zero-order a_u and b_u contributions to the upper eigenstate. For example, the intensity of the transitions to the Δ_u level at 3860 cm^{-1} in the pure-bend polyad set $\{N_s, N_{res}\} = \{0, 6\}$ and at 5770 cm^{-1} in the stretch-bend polyad $\{1, 9\}$ arises from constructive interference with the admixed $3^n 4^1$ character. Thus the relative intensity decreases with n.

The emission to $N_{res} = 12$, shown in Figure 3 panels c and f, is qualitatively different because $v_4'' = 11$ is the location of the first node in the *trans*-bending progression from $3^2 6^1$, so the set of pure bending polyads with $\{N_s, N_{res}\} = \{0, 12\}$ do not appear in the spectrum from $3^2 6^1$. On the other hand, the *trans*-bending progression from $3^3 6^1$ has its first node in the *trans* bending progression at $v_4'' = 9$, so both the $\{2, 12\}$ and $\{0, 12\}$ polyad sets appear in the spectrum. This shift in the node position reflects the shift in the first node of the upper state vibrational wavefunction along the *trans*-bend coordinate.

The DF spectrum to the $\{1, 11\}$ polyad set is shown in Figure 4 and is compared with both the results of the full Franck-Condon calculation, described in Refs. 24 and 25 (upward stick spectra) and the Cartesian propensity model described in Section III (downward stick spectra). The Cartesian propensity model does a fairly good job of reproducing the highly fractionated bright states, but the relative intensities at the weak, high-frequency end of the polyad are not reproduced by the model. For example, the model overestimates the intensity of the cluster at $\sim$7080 cm^{-1} relative to the peaks at $\sim$7220 cm^{-1}. When the full FC calculation is used, the relative intensities are in closer agreement with the observed spectrum. The cause for this is Duschinsky rotation among the b_u levels (ν_5' and ν_6', which correlate to ν_3'' and ν_5''—see Tables I-II). In the full FC calculation, there is non-negligible intensity into the class of bright states $(v_1, v_2, v_3, v_4^{(l_4)}, v_5^{(l_5)}) = (0, 0, 1, 6^{(l)}, 0^0)$. This class

of bright states involves an exchange of one quantum of ν_3'' for $\nu_2'' + \nu_4'' + \nu_5''$ and carries approximately 0.3% of the intensity away from the nominally bright states of the type $(0, 1, 0, 7^{(l_4)}, 1^{(l_5)})$, which is sufficient to cause noticeable disagreement with the model at the weak, high-frequency end of the polyad. In emission from $3^3 6^1$, the full FC calculation still places too much relative intensity in the cluster at ∼7120 cm^{-1}. This is probably caused by additional anharmonic interactions between $3^3 6^1$ and nearby levels (most notably B^5(II) $K = 1$).[10] At present, these interactions are incompletely understood and are not taken into account in our model.

Figure 1 shows the SEP spectra (downward peaks) from the three $K' = 1$ rotational stacks of the 3^2B^2 polyad. Roman numerals are used to label the admixed energy levels from low to high. Also shown for comparison are the DF spectrum from 3^2B^2(III) and the relative intensity patterns obtained from the Cartesian propensity model. The SEP spectra are obtained at much higher resolution than the DF spectrum, but the DF spectrum has greater sensitivity. Furthermore, the DF spectrum has its intensity calibrated against the emission spectrum of a halogen lamp dispersed to the same detector, whereas the intensities in the SEP spectra are not corrected for fluctuations in laser power and laboratory conditions as the laser is scanned. Therefore, the relative intensities in the DF spectrum are quantitatively accurate to within better than 15%, whereas the relative intensities in the SEP spectra are only qualitative.

The intensity patterns in Figure 1 are reproduced remarkably well by the Cartesian propensity model. The zero-order $3^2 6^2$ state is detuned from polyad resonance by isomerization-induced x_{36} cross anharmonicity so that it is separated from the zero-order $3^2 4^1 6^1$ level by 82.12 cm^{-1} and from the zero-order $3^2 4^2$ level by 102.91 cm^{-1}. As a result, the 3^2B^2(I) $J_{K_a K_c} = 1_{10}$ level escapes most of the effect of a-axis Coriolis interaction with $3^2 4^1 6^1$ via the $2A\zeta^a_{46} = 23.559$ cm^{-1} matrix element, but it is not immune to Darling-Dennison interaction with $3^2 4^2$ via the $K_{4466} = -66.502$ cm^{-1} matrix element (see Table IV).[5]

As a result of strong a-axis Coriolis interaction between $3^2 4^2$(a$_g$) and $3^2 4^1 6^1$(b$_g$), the emission spectra from 3^2B^2(II) and 3^2B^2(III) both terminate on levels with Σ_g^+ and Σ_g^- symmetry with comparable relative intensity, even though $3^2 4^2$(a$_g$) nominally fluoresces only to $l = 0$ levels of Σ_g^+ symmetry and $3^2 4^1 6^1$(b$_g$) fluoresces only to $l = 0$ levels of Σ_g^- symmetry. On the other hand, the emission spectrum from 3^2B^2(I) includes fluorescence only to $l = 0$ levels of Σ_g^+ symmetry, because $3^2 6^2$ is detuned from a-axis Coriolis resonance

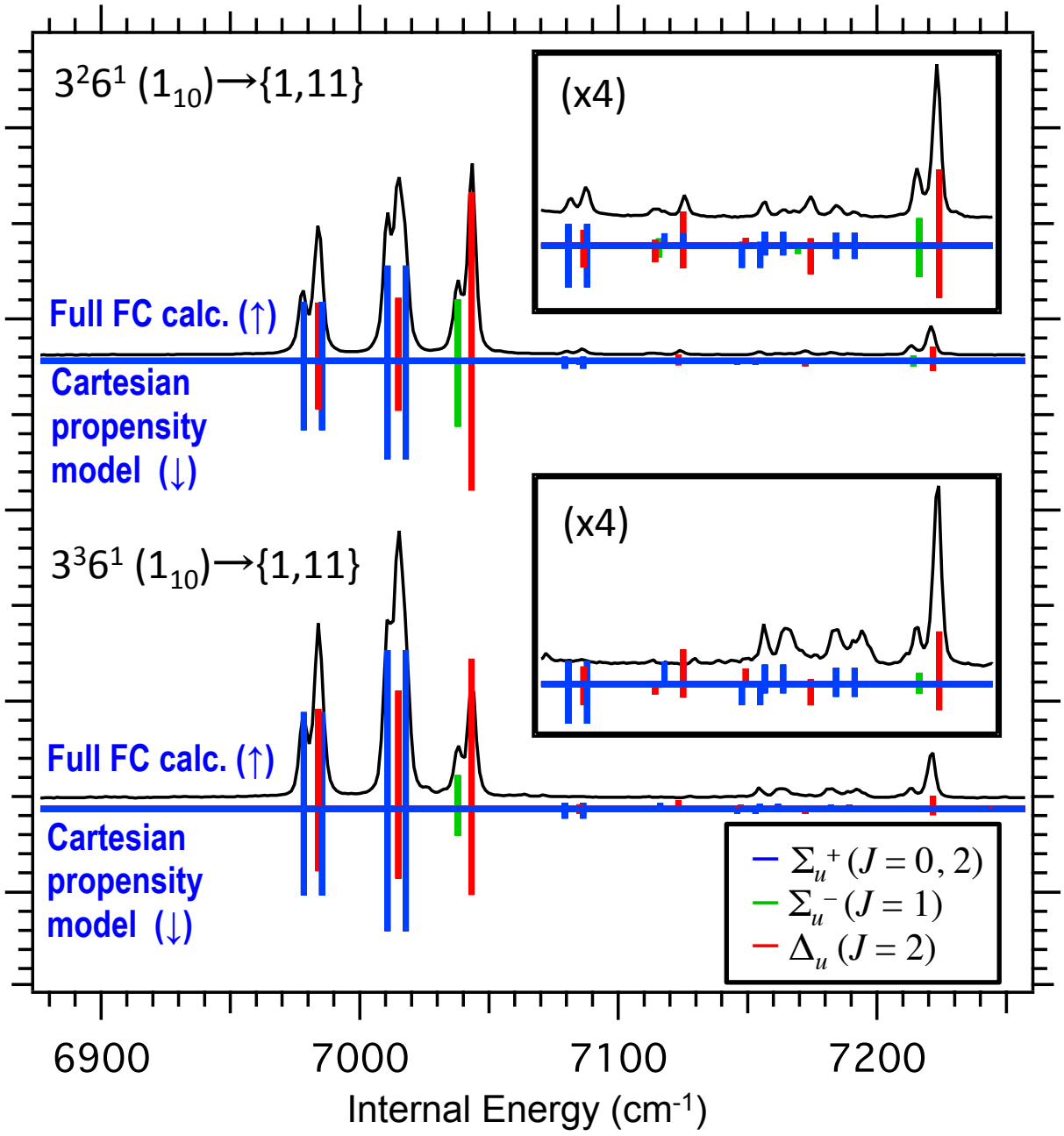

FIG. 4. High-resolution DF spectra obtained from $J_{K_a K_c} = 1_{10}$ rotational levels of $3^2 6^1$ and $3^3 6^1$ into the $\{N_s, N_{\rm res}\} = \{1, 11\}$ polyad set. The DF spectra have been previously reported in Ref. 15. For comparison, the relative intensities obtained from the Cartesian propensity model (downward stick spectra) and the Full Franck-Condon calculation described in Ref. 24 (upward stick spectra) are shown, colored according to the vibrational symmetry of the lower level (see legend). Duschinsky rotation of the b_u modes leads to minor discrepancies between the observed spectrum and the Cartesian propensity model, which are reproduced by using the Full FC calculation. (See the text for further discussion.)

with $3^2 4^1 6^1$. In the emission spectrum from 3^2B^2(III), the first cluster at $\sim$6380 cm^{-1} is absent due to destructive interference from $3^2 4^2 \leftrightarrow 3^2 6^2$ Darling-Dennison interaction. Unfortunately, the SEP spectrum obtained from 3^2B^2(I) has poor signal-to-noise due to the weakness of the PUMP transition, so the complementary constructive interference is not observed in the spectrum. Nevertheless, the six peaks in the 3^2B^2(I) SEP spectrum that are above the signal-to-noise floor are the six strongest transitions predicted by the Cartesian propensity model.

VI. ANALOGY TO NONLINEAR MOLECULAR SYSTEMS

Our goal in the current work has been to model the emission spectrum of acetylene, but in this section we briefly point out that our analysis is generally applicable to a wide range of molecular systems. In any electronic transition that involves a change of equilibrium geometry from a point group with degenerate representations to one without degenerate representations, each doubly-degenerate vibrational mode will correlate with two non-degenerate vibrational modes of different symmetry. Therefore, we expect similar effects not only in other linear-to-bent transitions but also in any other symmetric-to-asymmetric-top transitions, where the coordinate transformations for Franck-Condon integrals are most naturally performed using a Cartesian basis for the degenerate vibrations.

As a concrete example, consider the doubly degenerate mode ν''_{11} in the ground electronic state of allene $^1A_1$ (D_{2d}), pictured in the bottom half of Figure 5. Because allene is a symmetric top in the D_{2d} configuration, the choice of molecule-fixed x and y axes is arbitrary and any linear combination of the degenerate components may be used to represent the vibration. In Figure 5, we have chosen the x and y axes to lie in the planes defined by the H–C–H groups at either end of the molecule, which are oriented at 90° to one another. We have chosen the phases of the two components so that ν''_{11x} encodes motion in the xz plane and ν''_{11y} encodes motion in the yz plane. In either case, one of the H–C–H groups undergoes an out-of-plane rocking motion and the other H–C–H group undergoes an in-plane wagging motion. In the rotating allene molecule, the components of the degenerate e vibrational modes are split by first-order (and higher-order) a-axis Coriolis interactions into eigenstates with well-defined l quantum number.[37] Eigenstates of this type with $\pm l_{11}$ vibrational angular momentum quantum number will have wavefunctions that depend on

the complex linear combination of Cartesian normal coordinates $q''_{11x} \pm iq''_{11y}$.

The first excited $^1B_1$ electronic state of allene is stabilized by a large-amplitude torsion according to Walsh's rules, and theoretical calculations predict a planar geometry.[38] (The electronic symmetry correlates to ^1A_g in D_{2h}.) The doubly-degenerate e vibrational modes are split into singly degenerate modes of b_2 and b_3 symmetry. The top half of Figure 5 shows the $\nu'_{14}(b_{3u})$ and $\nu'_{15}(b_{2u})$ modes that correlate with the y- and x-axis components of ν''_{11y} and ν''_{11x}, respectively. Although similar correlations exist for the other doubly degenerate modes of allene, we have chosen this mode as an example because it bears a striking resemblance to the acetylene case where out-of-plane torsion (ν'_4) and in-plane bending (ν'_6) modes in the excited electronic state correlate with the Cartesian components of the degenerate ground electronic state *cis* bend (ν''_5).

In analogy to acetylene, we expect the Franck-Condon factors to obey propensity rules in the basis of the *Cartesian* components of ν''_{11}. That is, we expect bright states that conserve quanta of $v''_{11y} = v'_{14}$ and $v''_{11x} = v'_{15}$ to have the strongest Franck-Condon factors. These zero-order Cartesian bright states will be fractionated by the effective Hamiltonian into eigenstates with well-defined vibrational angular momentum. Certainly, this is not a novel idea, because the natural approach to the coordinate transformation the in planar↔twisted allene problem is to use the point group of lower symmetry (D_{2h}). The authors of Ref. 39 have used *ab initio* calculations of the ground $^1A_1$ and excited ^1A_g electronic states to calculate a full-dimensional Duschinsky matrix for the transition. The results indicate that the q'_{14} and q'_{15} modes remain essentially unmixed with other normal coordinates, which supports our argument for Cartesian propensity rules. In Table 5 of Ref. 39, the relative orientations of the x- and y- axes for the ground state Cartesian-to-normal-mode transformation are not specified (and the choice is arbitrary for symmetric top molecules), but the normal coordinates will match those given in our Figure 5 if the axes are chosen to lie in the dihedral planes (rotated 45° about the z-axis relative to our axis choice in Figure 5).

There are numerous double-bonded systems that undergo torsional displacement upon electronic excitation and similar propensity arguments should hold. Such systems have received widespread attention because of interest in photoinduced *cis-trans* isomerization.[40] Propensities will exist for conserved quanta in Cartesian Franck-Condon zero-order bright states to be fractionated among the eigenstates by Coriolis forces and other interactions. Of course, the zero-order Franck-Condon bright states have a direct bearing on photoinduced

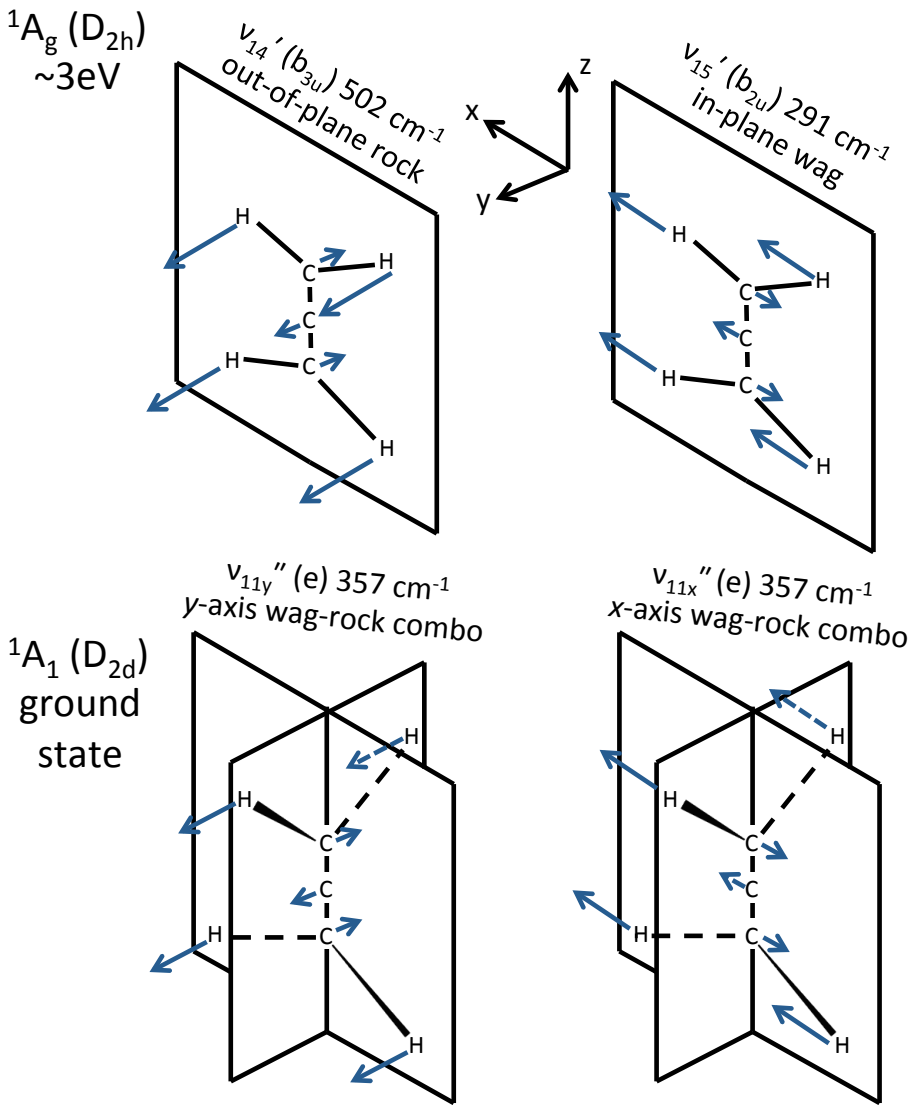

FIG. 5. Allene has a twisted D_{2d} geometry in its $^1A_1$ ground state but $\pi^* \leftarrow \pi$ excitation leads to a planar D_{2h} ^1A_g state at an adiabatic (non-vertical) electronic excitation energy of ~3 eV. The lower half of the figure depicts the two Cartesian components of the degenerate ν_{11}'' (e) vibrational mode. These components correlate to the non-degenerate out-of-plane rock ν_{14}' and in-plane wag ν_{15}' of the excited state.

isomerization dynamics.

VII. DISCUSSION AND CONCLUSION

Although the $\tilde{A} \rightarrow \tilde{X}$ emission intensities in acetylene have attracted the attention of researchers for more than two decades, the origin of relative intensities within polyad sets with given $\{N_s, N_{\rm res}\}$ quantum numbers have not previously been fully understood. For

example, the authors of Ref. 15 were forced to treat the interference pattern of Δ_u levels in the 3^n6^1 DF spectra by empirical fitting—it was not understood at the time how to predict the interferences, even though the eigenstate compositions of the upper levels[7] and the lower levels[15,35] were already known. So far, fluorescence patterns obtained from $\tilde{\mathrm{A}}$-state levels with intensity in B^n polyads have always been discussed in terms of *more than one* bright state per polyad of the $\tilde{\mathrm{X}}$ state, because the $\tilde{\mathrm{X}}$-state effective Hamiltonian is written in terms of the polar 2DHO basis.[15] In the current work, we demonstrate that in the *Cartesian* basis of degenerate 2DHOs for the bending modes, this is *not* the case, and there is a propensity for *only one* bright state per $\tilde{\mathrm{X}}$-state polyad, described in Eq. (8). In other words, we show that the most appropriate basis for writing the effective Hamiltonian of the linear $\tilde{\mathrm{X}}$ state (the polar basis) is *not the same* as the "best" basis for describing the zero-order bright states that are observed in emission from the $\tilde{\mathrm{A}}$ state. These are better described in the Cartesian basis because of the way in which the bent $\tilde{\mathrm{A}}$ state "chooses" an x, y axis frame for Franck-Condon integral. However, the two basis sets are connected by a straightforward ladder operator transformation that enables us to greatly simplify our interpretation of the intensity patterns.

Our treatment of the linear-to-bent acetylene transition is analogous to the most natural treatment for nonlinear symmetric-to-asymmetric-top transitions, where the x and y components of degenerate symmetric top vibrations are chosen to correlate to the components of the lower-symmetry modes along the well-defined x and y asymmetric top axes. However, linear-to-bent transitions have led to confusion in the literature because the number of vibrational degrees of freedom changes from $3N-5$ to $3N-6$, so the correlation of the bending modes is not straightforward. We believe that our treatment should be quite general for linear polyatomic molecules undergoing transitions to bent geometries. One Cartesian bending mode component will correlate to the a-axis rotation in the bent molecule. Due to Eckart constraints, this component will not contribute to the vibrational FC overlap. Franck-Condon propensities in the other bending modes should be viewed in the basis of in-plane vs. out-of-plane Cartesian components of the planes chosen by the nonlinear equilibrium configuration.

Furthermore, the relative intensities *between* the different polyads that comprise a polyad set with given $\{N_s, N_{\mathrm{res}}\}$ quantum numbers (but differing in l, g/u symmetry and $+/-$ total parity) are also correctly described by the Cartesian propensity model. Of course, in order

to predict the relative intensities between polyad sets differing in N_s and $N_{\rm res}$, one must also know the Franck-Condon progressions in the FC-active modes, ν_2'' and ν_4''. A full FC treatment is also necessary in order to correct for the effects of Duschinsky rotation or for interferences caused by $\tilde{\rm A}$-state interactions that are off-diagonal in the approximately conserved B^n polyads. The effects of Duschinsky rotation are minor and will not affect emission intensities into pure bending polyads because each of the $\tilde{\rm A}$-state bending modes (ν_3', ν_4', and ν_6') belong to different symmetry blocks, so Duschinsky rotation only causes stretch↔stretch or stretch↔bend interactions, and *not* bend↔bend interactions. However, in the absence of a global rovibrational $\tilde{\rm A}$-state effective Hamiltonian, *extrapolyad* interactions remain a challenge.

The success of our Cartesian propensity model relies on our knowledge of the B^n intrapolyad interactions in the $\tilde{\rm A}$ state. Not only does the model provide an additional physical test of our description of intra-polyad interactions in the upper levels—it should also provide us with a means of observing directly the evolution of the bending dynamics of $\tilde{\rm A}$-state acetylene in the vicinity of the *trans* ⇌ *cis* isomerization. For example, Figure 4 of Ref. 41 depicts the evolution of the 3^nB^4 polyad wavefunctions as quanta of ν_3' are added. Intrapolyad Darling-Dennison resonance causes the wavefunctions of B^4 to resemble degenerate 2DHO wavefunctions with well-defined l quantum number. However, as quanta in ν_3' are added, the isomerization causes the bending character to evolve in a manner that ought to be directly observable in the emission patterns from these levels. Previous work has made qualitative use of intensity distributions in overview DF spectra to characterize levels of $\tilde{\rm A}$-state acetylene.[14,42] However, as we have shown in the current work, the full emission spectrum is not necessary—the high-resolution emission pattern from the upper level in question to a single $\tilde{\rm X}$-state polyad set provides the quantitative information necessary for a complete characterization of the bending dynamics of the upper level.

Finally, the Cartesian propensity model gives us an additional tool for understanding the vibrational dynamics in the $\tilde{\rm X}$-state that are encoded by the intrapolyad fractionation patterns that are observed in the spectrum, since it is straightforward to transform from a Cartesian zero-order bright state to a spectral interference pattern. As shown in Ref. 25, it is also straightforward to transform to the basis of local bending modes relevant to the acetylene ⇌ vinylidene isomerization. Indeed, the quest to find $\tilde{\rm A}$-state levels that grant access to local bending levels along the acetylene-vinylidene isomerization path was a major

motivating factor for the work described here.

VIII. ACKNOWLEDGEMENTS

We are indebted to Prof. Kaoru Yamanouchi and Dr. Richard Duan for sharing their raw DF data with us. GBP would like to thank P. Bryan Changala for stimulating discussions. This material is based upon work supported by the U.S. Department of Energy, Office of Science, Chemical Sciences Geosciences and Biosciences Division of the Basic Energy Sciences Office, under Award Number DE-FG0287ER13671.

REFERENCES

[1]King, G. W.; Ingold, C. K. The Bent Excited State of Acetylene. *Nature* **1952**, *169*, 1101–1102.

[2]Ingold, C. K.; King, G. W. Excited states of acetylene. *J. Chem. Soc.* **1953**, *1953*, 2702–2755.

[3]Innes, K. K. Analysis of the Near Ultraviolet Absorption Spectrum of Acetylene. *J. Chem. Phys.* **1954**, *22*, 863–876.

[4]Jacobson, M. P.; Field, R. W. Acetylene at the Threshold of Isomerization. *J. Phys. Chem. A* **2000**, *104*, 3073–3086.

[5]Steeves, A. H.; Bechtel, H. A.; Merer, A. J.; Yamakita, N.; Tsuchiya, S.; Field, R. W. Stretch-bend combination polyads in the $\tilde{A}\ ^1A_u$ state of acetylene, C_2H_2. *J. Mol. Spectrosc.* **2009**, *256*, 256–278.

[6]Utz, A. L.; Tobiason, J. D.; Carrasquillo M., E.; Sanders, L. J.; Crim, F. F. The direct observation, assignment, and partial deperturbation of the ν_4 and ν_6 vibrational fundamentals in $\tilde{A}?^1A_u$ acetylene (C_2H_2). *J. Chem. Phys.* **1993**, *98*, 2742–2753.

[7]Mizoguchi, M.; Yamakita, N.; Tsuchiya, S.; Iwasaki, A.; Hoshina, K.; Yamanouchi, K. IR-UV Double Resonance Spectroscopy of Acetylene in the $\tilde{A}\ ^1A_u$ $n\nu_3' + \nu_4'$ and $n\nu_3' + \nu_6'$ $(n = 2, 3)$ *Ungerade* Vibrational States. *J. Phys. Chem. A* **2000**, *104*, 10212–10219.

[8]Merer, A. J.; Yamakita, N.; Tsuchiya, S.; Steeves, A. H.; Bechtel, H. A.; Field, R. W. Darling-Dennison resonance and Coriolis coupling in the bending overtones of the $\tilde{A}\ ^1A_u$ state of acetylene, C_2H_2. *J. Chem. Phys.* **2008**, *129*, 054304.

[9]Merer, A. J.; Steeves, A. H.; Baraban, J. H.; Bechtel, H. A.; Field, R. W. *Cis-trans* isomerization in the S_1 state of acetylene: Identification of *cis*-well vibrational levels. *J. Chem. Phys.* **2011**, *134*, 244310.

[10]Baraban, J. H.; Changala, P. B.; Merer, A. J.; Steeves, A. H.; Bechtel, H. A.; Field, R. W. The $\tilde{A}\ ^1A_u$ state of acetylene: *Ungerade* vibrational levels in the region 45,800–46,550 cm^{-1}. *Mol. Phys.* **2012**, *110*, 2707–2723.

[11]Jiang, J.; Baraban, J. H.; Park, G. B.; Clark, M. L.; Field, R. W. Laser-Induced Fluorescence Study of the S_1 State of Doubly-Substituted ^{13}C Acetylene and Harmonic Force Field Determination. *J. Phys. Chem. A* **2013**, *117*, 13696–13703.

[12]Solina, S. A. B.; O'Brien, J. P.; Field, R. W.; Polik, W. F. Dispersed Fluorescence Spectrum of Acetylene from the $\tilde{A}\ ^1A_u$ Origin: Recognition of Polyads and Test of Multiresonant Effective Hamiltonian Model for the $\tilde{X}$ State. *J. Phys. Chem.* **1996**, *100*, 7797–7809.

[13]Jacobson, M. P.; O'Brien, J. P.; Field, R. W. Anomalously slow intramolecular vibrational redistribution in the acetylene $\tilde{X}?^1\Sigma_g^+$ state above 10?000 cm^{-1} of internal energy. *J. Chem. Phys.* **1998**, *109*, 3831–3840.

[14]Tsuji, K.; Terauchi, C.; Shibuya, K.; Tsuchiya, S. *Trans-cis* isomerization of acetylene in the $\tilde{A}\ ^1A_u$ state as studied by dispersed fluorescence spectroscopy. *Chem. Phys. Lett.* **1999**, *306*, 41–47.

[15]Hoshina, K.; Iwasaki, A.; Yamanouchi, K.; Jacobson, M. P.; Field, R. W. The infrared-ultraviolet dispersed fluorescence spectrum of acetylene: New classes of bright states. *J. Chem. Phys.* **2001**, *114*, 7424–7442.

[16]Yamanouchi, K.; Ikeda, N.; Tsuchiya, S.; Jonas, D. M.; Lundberg, J. K.; Adamson, G. W.; Field, R. W. Vibrationally highly excited acetylene as studied by dispersed fluorescence and stimulated emission pumping spectroscopy: Vibrational assignment of the feature states. *J. Chem. Phys.* **1991**, *95*, 6330–6342.

[17]Jonas, D. M.; Solina, S. A. B.; Rajaram, B.; Silbey, R. J.; Field, R. W.; Yamanouchi, K.; Tsuchiya, S. Intramolecular vibrational relaxation and forbidden transitions in the SEP spectrum of acetylene. *J. Chem. Phys.* **1992**, *97*, 2813–2816.

[18]Jacobson, M. P.; Silbey, R. J.; Field, R. W. Local mode behavior in the acetylene bending system. *J. Chem. Phys.* **1999**, *110*, 845–859.

[19]Tyng, V.; Kellman, M. E. Bending Dynamics of Acetylene: New Modes Born in Bifurcations of Normal Modes. *J. Phys. Chem. B* **2006**, *110*, 18859–18871.

[20]Baraban, J. H.; Beck, A. R.; Steeves, A. H.; Stanton, J. F.; Field, R. W. Reduced dimension discrete variable representation study of *cis-trans* isomerization in the S_1 state of C_2H_2. *J. Chem. Phys.* **2011**, *134*, 244311.

[21]Wong, B. M.; Steeves, A. H.; Field, R. W. Electronic Signatures of Large Amplitude Motions: Dipole Moments of Vibrationally Excited Local-Bend and Local-Stretch States of S_0 Acetylene. *J. Phys. Chem. B* **2006**, *110*, 18912–18920.

[22]Joseph, S.; Varandas, A. J. C. Accurate MRCI and CC Study of the Most Relevant Stationary Points and Other Topographical Attributes for the Ground-State C_2H_2 Potential Energy Surface. *J. Phys. Chem. A* **2010**, *114*, 13277–13287.

[23]Han, H.; Li, A.; Guo, H. An *ab initio* based near spectroscopically accurate global potential energy surface for the acetylene-vinylidene isomerization. *J. Chem. Phys.* **2014**, (accepted).

[24]Park, G. B. Full dimensional Franck-Condon factors for the acetylene $\tilde{A}\ ^1A_u$–$\tilde{X}\ ^1\Sigma_g^+$ transition. I. Method for calculating polyatomic linear-bent vibrational intensity factors and evaluation of calculated intensities for the *gerade* vibrational modes in acetylene. *J. Chem. Phys.* **2014**, *141*, 134304.

[25]Park, G. B.; Baraban, J. H.; Field, R. W. Full dimensional Franck-Condon factors for the acetylene $\tilde{A}\ ^1A_u$–$\tilde{X}\ ^1\Sigma_g^+$ transition. II. Vibrational overlap factors for levels involving excitation in *ungerade* modes. *J. Chem. Phys.* **2014**, *141*, 134305.

[26]Temsamani, M. A.; Herman, M. The vibrational energy levels in acetylene 12C2H2: Towards a regular pattern at higher energies. *The Journal of Chemical Physics* **1995**, *102*, 6371–6384.

[27]Temsamani, M. A.; Herman, M.; Solina, S. A. B.; O'Brien, J. P.; Field, R. W. Highly vibrationally excited 12C2H2 in the ?? 1+g state: Complementarity of absorption and dispersed fluorescence spectra. *The Journal of Chemical Physics* **1996**, *105*, 11357–11359.

[28]Jacobson, M. P.; O'Brien, J. P.; Silbey, R. J.; Field, R. W. Pure bending dynamics in the acetylene ??1?g+ state up to 15?000 cm?1 of internal energy. *The Journal of Chemical Physics* **1998**, *109*, 121–133.

[29]El Idrissi, M. I.; Liévin, J.; Campargue, A.; Herman, M. The vibrational energy pattern in acetylene (IV): Updated global vibration constants for $^{12}C_2H_2$. *J. Chem. Phys.* **1999**, *110*, 2074–2086.

[30]O'Brien, J. P.; Jacobson, M. P.; Sokol, J. J.; Coy, S. L.; Field, R. W. Numerical pattern recognition analysis of acetylene dispersed fluorescence spectra. *J. Chem. Phys.* **1998**, *108*,

7100–7113.

[31]Steeves, A. H. Electronic Signatures of Large Amplitude Motions. Ph.D. thesis, Massachusetts Institute of Technology, 2009.

[32]Kovner, M. A.; Gorokhov, A. V.; Gerasimov, G. A.; Bazarov, E. N. Calculation of the Franck-Condon Integrals for a Triatomic Molecule. The $^1B_2 \rightarrow ^1\Sigma_g^+$ Transition in the CO_2 Molecule. *Opt. Spectrosc.* **1970**, *29*, 356–359.

[33]Watson, J. K. G. Vibration-rotation Hamiltonians of linear molecules. *Mol. Phys.* **1993**, *79*, 943–951.

[34]Watson, J. K. G. Calculated Vibrational Intensities in the $\tilde{A}$-$\tilde{X}$ Electronic Transition of Acetylene. *J. Mol. Spectrosc.* **2001**, *207*, 276–284.

[35]Herman, M.; Campargue, A.; Idrissi, M. I. E.; Auwera, J. V. Vibrational Spectroscopic Database on Acetylene, $\tilde{X}\ ^1\Sigma_g^+$ ($^{12}C_2H_2$, $^{12}C_2D_2$, and $^{13}C_2H_2$). *J. Phys. Chem. Ref. Data* **2003**, *32*, 921–1361.

[36]Merer, A. J.; Duan, Z.; Field, R. W.; Watson, J. K. G. Perturbations in the $4\nu_3$ level of the $\tilde{A}\ ^1A_u$ state of acetylene, C_2H_2. *Can. J. Phys.* **2009**, *87*, 437–441.

[37]Mills, I.; Smith, W.; Duncan, J. Coriolis perturbations in the infrared spectrum of allene. *J. Mol. Spectrosc.* **1965**, *16*, 349–377.

[38]Jackson, W. M.; Mebel, A. M.; Lin, S. H.; Lee, Y. T. Using *ab Initio* MO Calculations To Understand the Photodissociation Dynamics of CH_2CCH_2 and CH_2C_2. *J. Phys. Chem. A* **1997**, *101*, 6638–6646.

[39]Mebel, A. M.; Hayashi, M.; Liang, K. K.; Lin, S. H. *Ab Initio* Calculations of Vibronic Spectra and Dynamics for Small Polyatomic Molecules: Role of Duschinsky Effect. *J. Phys. Chem. A* **1999**, *103*, 10674–10690.

[40]Altoæ, P.; Bernardi, F.; Conti, I.; Garavelli, M.; Negri, F.; Orlandi, G. Light driven molecular switches: Exploring and tuning their photophysical and photochemical properties. *Theor. Chem. Acc.* **2007**, *117*, 1041–1059.

[41]Changala, P. B.; Baraban, J. H.; Stanton, J. F.; Merer, A. J.; Field, R. W. Reduced dimension rovibrational variational calculations of the S_1 state of C_2H_2. II. The S_1 rovibrational manifold and the effects of isomerization. *J. Chem. Phys.* **2014**, *140*, 024313.

[42]Duan, Z. Spectroscopic Study of the Acetylene Species. Ph.D. thesis, Massachusetts Institute of Technology, 2003.

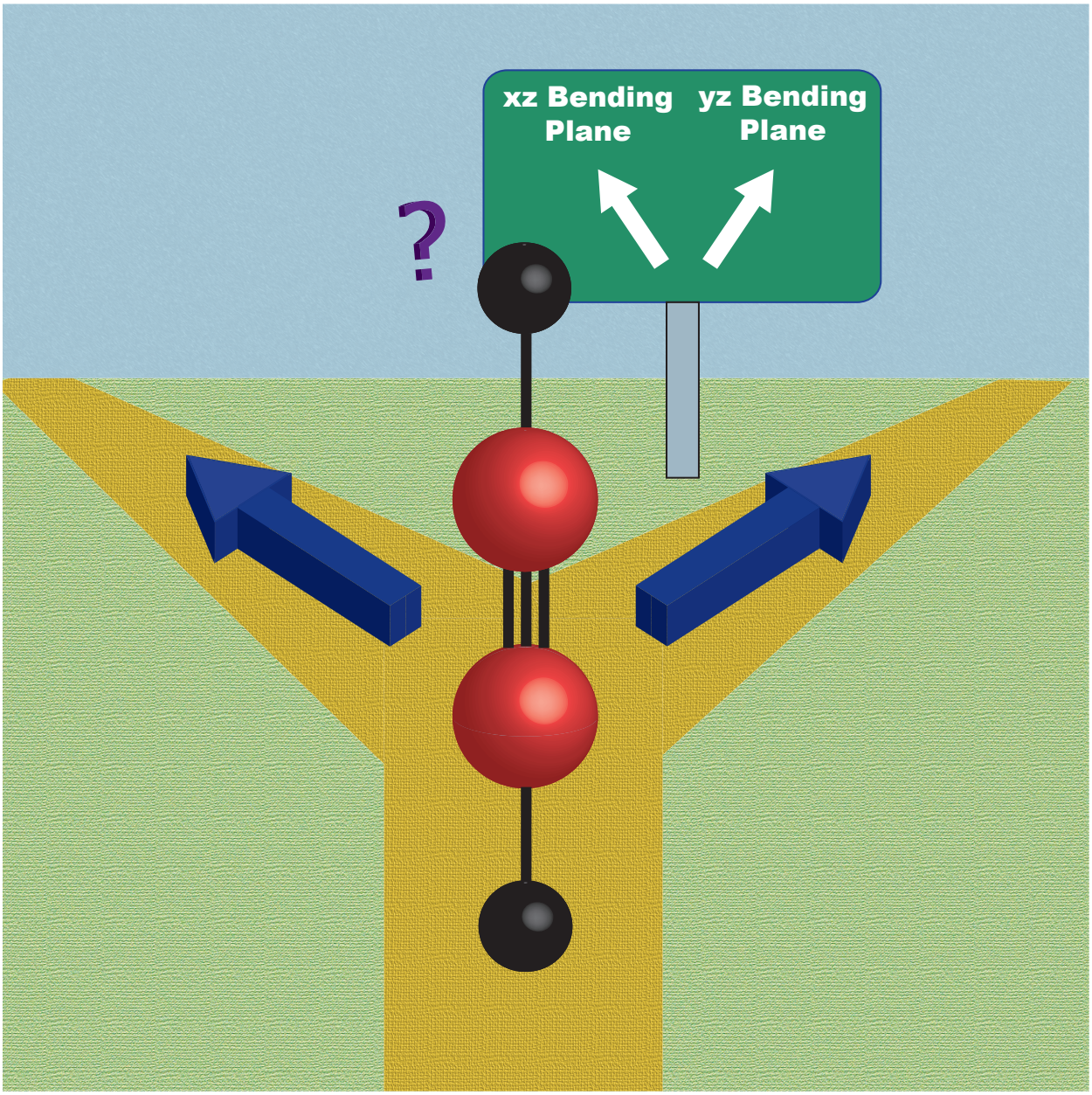

FIG. 6. Table of Contents Image